

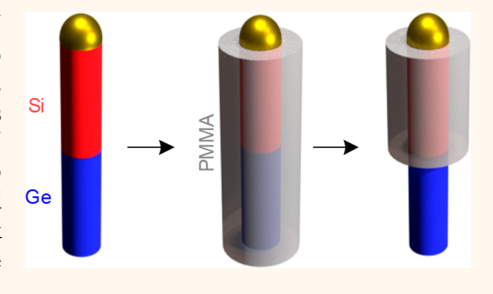
Bottom-Up Masking of Si/Ge Surfaces and Nanowire Heterostructures via Surface-Initiated Polymerization and Selective Etching

Amar T. Mohabir, Gozde Tutuncuoglu, Trent Weiss, Eric M. Vogel, and Michael A. Filler*,

[†]School of Chemical & Biomolecular Engineering, Georgia Institute of Technology, Atlanta, Georgia 30332, United States [‡]School of Materials Science & Engineering, Georgia Institute of Technology, Atlanta, Georgia 30332, United States

Supporting Information

ABSTRACT: The fully bottom-up and scalable synthesis of complex micro/ nanoscale materials and functional devices requires masking methods to define key features and direct the deposition of various coatings and films. Here, we demonstrate selective coaxial lithography via etching of surfaces (SCALES), an enabling bottom-up process to add polymer masks to micro/ nanoscale objects. SCALES is a three-step process, including (1) bottom-up synthesis of compositionally modulated structures, (2) surface-initiated polymerization of a conformal mask, and (3) selective removal of the mask only from regions whose underlying surface is susceptible to an etchant. We demonstrate the key features of and characterize the SCALES process with a



series of model Si/Ge systems: Si and Ge wafers, Si and Ge nanowires, and Si/Ge heterostructure nanowires.

KEYWORDS: bottom-up, polymer brush, pattern, semiconductor, nanowire, heterostructure

t is now possible to synthesize a variety of structures where composition is controlled with micro/nanoscale spatial precision. One well-known technique is the vaporliquid-solid (VLS) mechanism, which leverages a liquid seed nanoparticle to collect and concentrate precursors from the vapor to grow a solid nanowire. 1-3 Temporal control of precursor identity and delivery rate permits the programming of composition along the nanowire's length. 4-6 Subsequent deposition of thin films (e.g., dielectrics and metal electrodes) on these compositionally modulated structures can produce a variety of functional devices (e.g., transistors, sensors, waveguides, and solar cells).^{7–10} To date, the controlled placement of conformal coatings has been achieved by combining conventional photo or e-beam lithography with thin film deposition and lift-off. However, the utility of such top-down techniques outside of the laboratory is likely limited. Achieving the same degree of nanoscale complexity in a fully bottom-up fashion¹¹ promises to increase device manufacturing throughput.

Area-selective deposition (ASD) methods, in principle, offer a bottom-up route to selectively deposit films only in desired regions. 12-15 ASD can be accomplished in either an (1) intrinsic and/or (2) extrinsic manner. Intrinsic ASD leverages surface compositional or structural differences to achieve selectivity. 16,17 Because intrinsic ASD depends on the microscopic details of two or more surfaces, it is highly materials specific.¹⁷ Extrinsic ASD uses masks in the form of polymers¹⁸ or self-assembled monolayers (SAMs)¹³ to block deposition on certain surfaces. 18,19 The use of a separate material for masking, assuming a method exists for its deposition, results in a more versatile ASD process. To date, the creation of masks needed for extrinsic ASD has been accomplished using topdown lithographic methods. While useful in wafer-level processing,²⁰ such methods are not amenable to the scale-up of device manufacturing.

Here, we demonstrate a versatile bottom-up process, selective coaxial lithography via etching of surfaces (SCALES), to pattern micro/nanoscale objects with conformal polymer masks. Analogous to top-down lithography, the masks produced by SCALES promise to block and, in doing so, spatially control thin film deposition. However, unlike topdown lithography, which is largely limited to 2-D substrates, SCALES allows masks to be produced in a highly scalable, bottom-up manner on 3-D objects. In this way, SCALES is much more akin to the protecting groups commonly used during chemical synthesis.

SCALES involves three key steps: (1) synthesis of chemically or structurally heterogeneous structures, (2) surface-initiated polymerization of a suitable masking material, and (3) selective removal of the masking material by selectively etching the underlying surface. We demonstrate key features of SCALES with a series of model Si/Ge systems, including

Received: June 4, 2019 Accepted: December 19, 2019 Published: December 19, 2019



282

planar Si and Ge substrates and homogeneous Si and Ge nanowires, and then apply this understanding to heterostructured Si/Ge nanowires. In all cases, atom transfer radical polymerization (ATRP) is used to grow a poly(methyl methacrylate) (PMMA) film from both Si (SiO_x) and Ge (GeO_x) regions. ^{21–25} Taking advantage of chemical differences between Si (SiO_x) and Ge (GeO_x), ^{26,27} a subsequent selective etch in H_2O_2 removes PMMA from Ge (GeO_x). The PMMA mask remains on the Si (SiO_x) region. While the present work focuses on Si/Ge systems, we emphasize that SCALES is applicable to any material system where methods exist to (1) synthesize materials/structures with compositional heterogeneity, (2) graft polymers to their surfaces, and (3) selectively etch those surfaces.

RESULTS AND DISCUSSION

We first demonstrate the SCALES process on planar Si and Ge substrates. Each step required to attach PMMA, schematically illustrated in Figure 1, can be followed with X-ray photoelectron spectroscopy (XPS) and is shown in Figure 2 for Si. The starting substrate exhibits only adventitious carbon after cleaning (Figure 2a-c). Following attachment of APTES, we observe N(1s) photoelectron peaks at 400.6 and 401.6 eV, indicating the presence of N-C and N-H bonds, respectively (Figure 2d-f). ^{28,29} The presence of a C-Br bond is confirmed

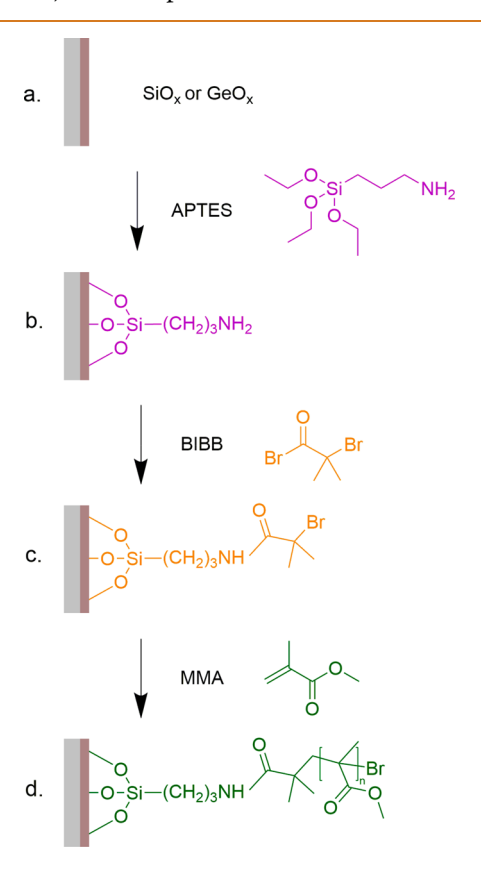


Figure 1. Surface-initiated polymerization illustration. (a) The starting surface is Si (SiO_x) or Ge (GeO_x). (b) 3-Aminopropyl triethoxysilane (APTES) is covalently attached to the oxide surfaces and serves as an anchoring group. (c) An initiator, α -bromoisobutyryl bromide (BIBB), is then reacted with the primary amine of APTES. (d) Poly(methyl methacrylate) (PMMA) is then grafted from the tertiary bromide of BIBB via atom transfer radical polymerization.

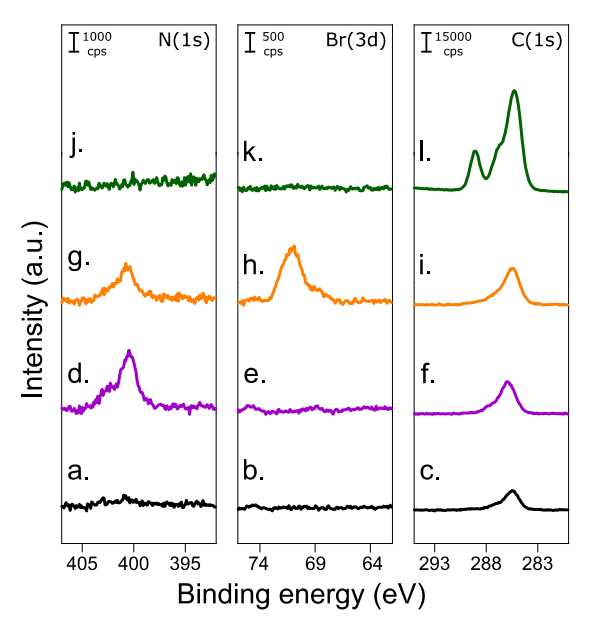


Figure 2. XPS characterization of surface-initiated polymerization. N(1s), Br(3d), and C(1s) photoelectron spectra for each step in the polymerization process (Figure 1) on a Si substrate: (a-c) Initial, native-oxide-covered substrate; (d-f) following APTES attachment; (g-i) following BIBB attachment; (j-l) following PMMA polymerization. The results are similar on a Ge substrate (not shown).

by the appearance of a Br(3d) photoelectron peak at 70.3 eV following BIBB attachment (Figure 2g-i).³⁰ Several strong C(1s) photoelectron peaks are present after PMMA polymerization. Peaks at 285.0, 286.8, and 289.1 eV are attributed to the C-C, C-O, and C=O bonds of PMMA, respectively (Figure 2j-l).^{31,32} We note, for the PMMA thicknesses studied here, that film thickness does not impact XPS peak intensity because we are electron escape depth limited.

The distinct chemical reactivity of SiO_x and GeO_x is next leveraged to selectively remove PMMA attached to the Ge substrate but not the Si substrate. Figure 3a and b show representative C(1s) photoelectron spectra of PMMA-coated Si and Ge substrates. After immersion of these substrates in H_2O_2 , Figure 3c reveals that the C(1s) photoelectron peak intensity is not affected for the Si substrate, but Figure 3d shows that it is sharply reduced for the Ge substrate. The weak C(1s) peak still observed on the Ge substrate after H_2O_2 etching is attributed to adventitious carbon and is quite distinct from the higher binding energy peaks representative of PMMA.³³

We now investigate the time scale for PMMA removal during H_2O_2 selective etching on Si and Ge substrates. Figure 4 shows integrated intensities of the C(1s), Si(2p), and Ge(3d) photoelectron peaks as a function of etch time (Supporting Information, Figures S1 and S2). Over the course of 60 min, Figure 4a shows that the C(1s) peak intensity remains largely unchanged for the Si substrate, while Figure 4b shows that it decreases markedly for the Ge substrate. The time scale for PMMA removal, defined here as the point where the C(1s) intensity for the Ge surface is reduced to 10% of its initial value, is approximately 30 min. Figure 4c and d show the trends for Si(2p) and Ge(3d) photoelectron peaks for the Si and Ge substrates, respectively. An increase in the Ge(3d) peak intensity for the Ge substrate is observed with time; however, little change is seen in the Si(2p) peak. The increase

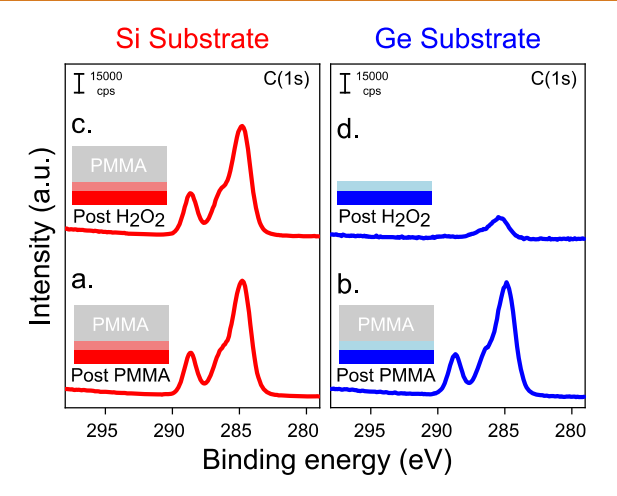


Figure 3. Selective removal of PMMA from planar Si and Ge substrates. C(1s) photoelectron spectra following PMMA polymerization on (a) Si (SiO_x) and (b) Ge (GeO_x) substrates. C(1s) photoelectron spectra following H_2O_2 selective etching of PMMA-grafted (c) Si (SiO_x) and (d) Ge (GeO_x) substrates. PMMA is selectively removed from the Ge substrate due to H_2O_2 attack of the underlying GeO_x/Ge . No discernible change is observed on the Si (SiO_x) substrate.

in Ge(3d) peak intensity is consistent with a decrease in the C(1s) peak intensity; removal of PMMA allows photoelectrons from the Ge substrate to reach the detector. Ellipsometric measurements of PMMA thickness as a function of H_2O_2 etch time on Si and Ge substrates are shown in Figure 4e and f, respectively. These data are consistent with our XPS measurements, also showing that PMMA removal only occurs on the Ge substrate during H_2O_2 exposure.

Our data suggest that polymer removal, as schematically illustrated in Figure 5, follows an etchant diffusion- or polymer transport-limited surface-reaction mechanism. Etchant molecules (i.e., H₂O₂) first diffuse to the substrate surface. Upon reaching the substrate surface to which PMMA is attached, the H₂O₂ etches the GeO_x surface layer on the Ge substrate but not the corresponding SiO, layer on the Si substrate. Upon GeO_x/Ge etching, the polymer detaches from the substrate and is transported into the etchant solution. With a Ge etch rate in H_2O_2 solution of ~0.3 monolayers/second, ³⁴ polymer release should be possible within a few seconds. However, as Figure 4 makes clear, polymer removal from the Ge surface occurs only after ~30 min. A study of polymer removal time as a function of initial polymer thickness displayed in Figure 6 reveals that removal time scales with starting polymer thickness. These data are consistent with a mechanism where surface reaction is fast and etchant diffusion through the polymer or polymer transport into the etchant solution limits the rate of the overall process. These relative rates are also consistent with the fact that H2O is a poor solvent for PMMA,³⁵ likely leading to both a contraction of the brush, reducing the H₂O₂ diffusion rate, and a reduced tendency for the PMMA to be solvated.

We now move on to a demonstration of the SCALES process on homogeneous Si and Ge nanowires. Figure 7a and b show SEM images of representative as-grown Si and Ge nanowires. Figure 7c and d show conformal PMMA films grafted from the SiO_x and GeO_x surface of the Si and Ge nanowires, respectively. For both types of nanowires, the PMMA film thickness is approximately 20 nm. The polymer

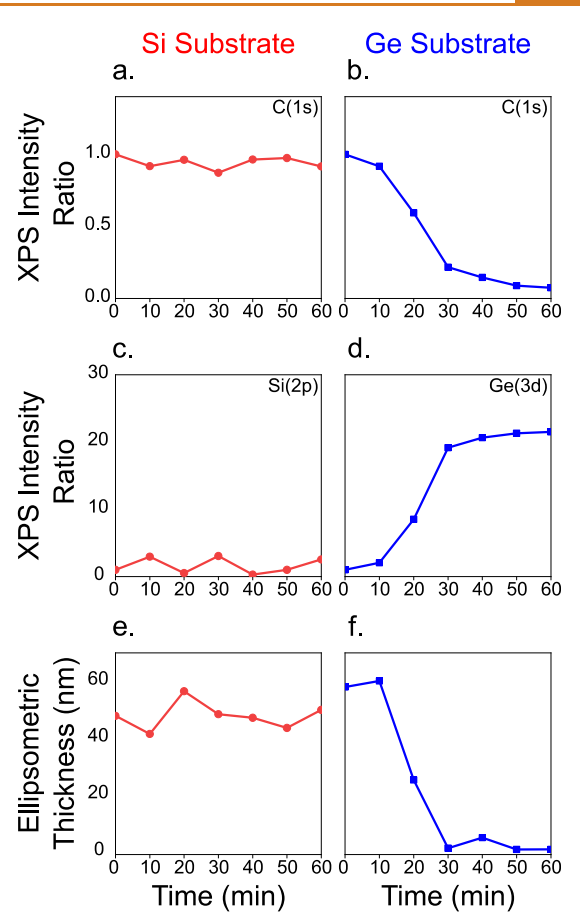


Figure 4. Transient studies of PMMA removal on planar Si and Ge substrates. C(1s) photoelectron peak integrated intensity ratioed to that at 0 min vs H_2O_2 etch time on (a) Si and (b) Ge substrates. (c) Si(2p) and (d) Ge(3d) photoelectron peak integrated intensity ratioed to that at 0 min vs H_2O_2 etch time on Si and Ge substrates, respectively. The decrease in C(1s) peak intensity and concomitant increase in Ge(3d) peak intensity for the Ge substrate, but not the Si substrate, indicate selective removal of PMMA. Ellipsometric thickness measurements of PMMA on a (e) Si and (f) Ge substrate vs H_2O_2 etch time reveal the same behavior.

also covers the Au seed particle. This observation is unsurprising, as the seed particle ejects semiconductor atoms (i.e., Si or Ge) atoms following growth, which then oxidize (i.e., to SiO_x or GeO_x) upon exposure to ambient. ³⁶ Figure 7e and f show the result of the H₂O₂ selective etch. The PMMA film remains on the Si nanowire but is removed from the Ge nanowire. While Figure 7f suggests polymer residue can sometimes remain on the Ge nanowire, scanning transmission electron microscopy (STEM) and energy dispersive X-ray (EDX) spectroscopy measurements show very little carbon (Supporting Information, Figure S4). Even if a small quantity of polymer were present, a variety of processes (e.g., mild oxygen plasma or rinsing in acetone) are likely able to remove it.³⁷ Furthermore, the seed particle on the Ge nanowire is almost always removed during the H2O2 etching. We suspect that this behavior results from GeO_x present at the Ge nanowire/seed particle interface that is rapidly etched in H_2O_2 . 38,39

The magnitude of the PMMA removal times differ between the planar substrates and nanowire cases, although they are within the same order of magnitude. The PMMA film is largely removed from Ge at ~ 30 and ~ 60 min in the planar substrate

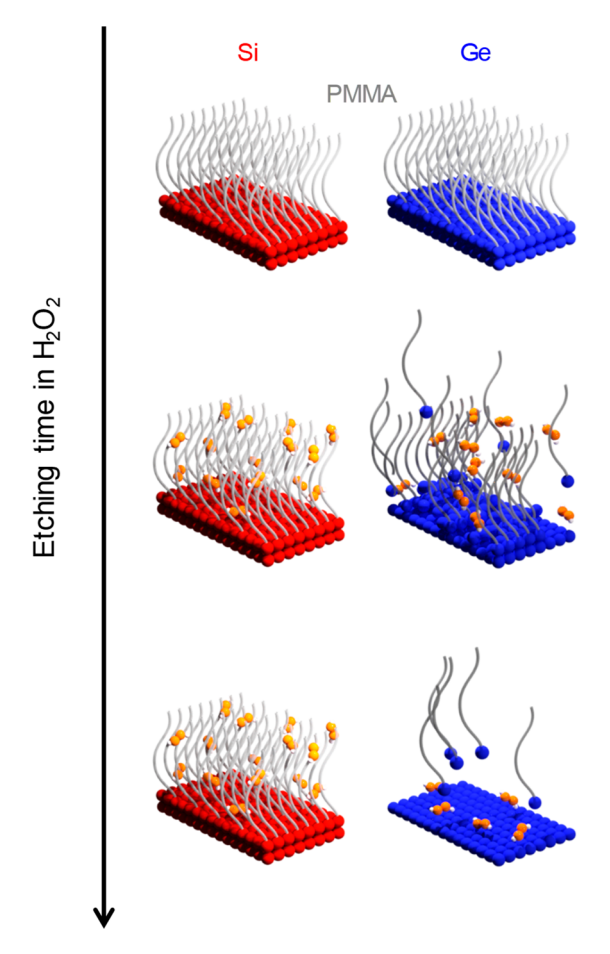


Figure 5. Proposed selective etching mechanism. H_2O_2 diffuses through the PMMA brush. When H_2O_2 reaches the underlying surface, it etches Ge (GeO_x). The PMMA covering Ge (GeO_x) is also removed with the atoms to which it is attached. Because H_2O_2 cannot etch Si (SiO₂), PMMA remains on that surface.

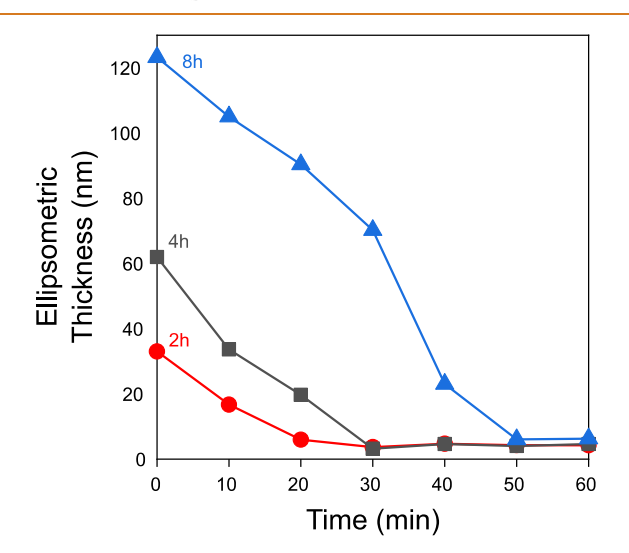


Figure 6. Polymer thickness dependent etch study. PMMA thickness as a function of H_2O_2 etching time for 2, 4, and 8 h polymerizations. These data show that polymer thickness correlates with etch time, indicating that SCALES is limited by etchant diffusion into the polymer or polymer transport into solution after surface etching.

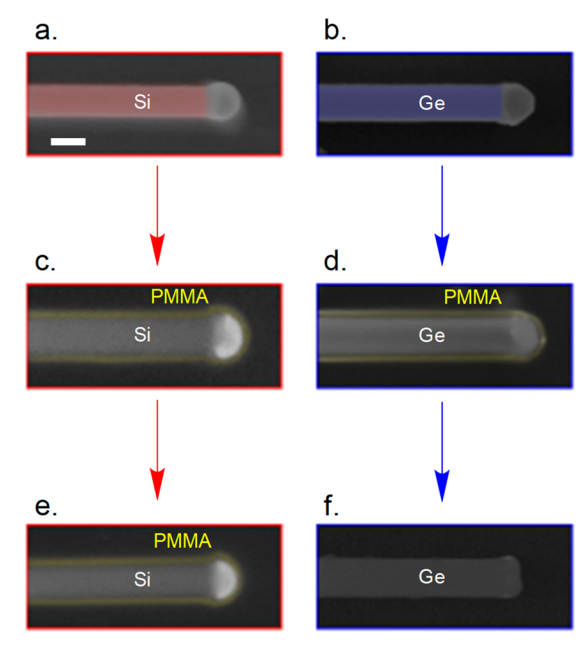


Figure 7. Demonstration of SCALES on homogeneous Si and Ge nanowires. SEM images of representative as-grown (a) Si and (b) Ge nanowires. Si and Ge are false-colored red and blue, respectively. SEM images of representative PMMA-grafted (c) Si and (d) Ge nanowires. PMMA is false-colored green for clarity. SEM images of representative PMMA-grafted (e) Si and (f) Ge nanowires following $\rm H_2O_2$ etching. PMMA is only removed from the Ge nanowire. Scale bar, 100 nm. The original, uncolored SEM images are shown in Figure S3.

and nanowire cases, respectively. Such a discrepancy is to be expected because of differences in substrate/nanowire surface structure and chemistry. For example, nanowire surfaces, depending on the details of growth and any postgrowth treatment, can be quite rough. Differences in surface roughness between planar substrates and nanowires likely modify parameters such as polymer graft density and result in differences in SCALES processing.

We combine our understanding of SCALES on planar substrates and homogeneous nanowires to demonstrate, as shown in Figure 8, the process for Si/Ge heterostructure nanowires. Figure 8a shows a SEM image of a representative as-grown Si/Ge heterostructure nanowire. We use a brief KOH etch to remove any Si atoms from the surface of the Ge segment, as shown in Figure 8b. We find this step to be necessary because a small amount of Si is likely deposited on the Ge segment during growth, which then oxidizes to SiO_x upon exposure to ambient. Without this brief KOH treatment, we are unable to remove PMMA from the Ge segment during H₂O₂ exposure. While KOH etches Ge (Figure 8b),⁴¹ we are confident that any unwanted Si is removed. Figure 8c shows a conformal PMMA film grafted to the Si/Ge heterostructure nanowire. The PMMA film thickness is approximately 20 nm, similar to that for the homogeneous nanowires (Figure 7c and d). Figure 8d shows the result of the selective H₂O₂ etch. As for prior substrate types, the Si segment retains the PMMA film, while the PMMA is removed from the Ge segment.

Work is currently underway in our laboratory to better understand the impact of key polymerization and selective etch parameters on the SCALES process. Polymer graft density and chain length, because they impact etchant diffusion and polymer entanglement, likely play a critical role. High graft

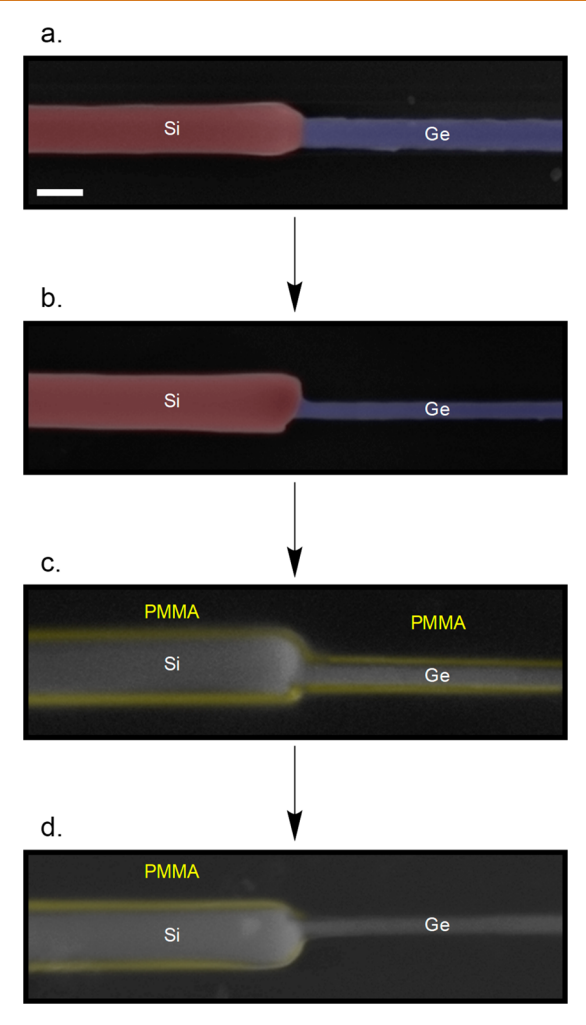


Figure 8. Demonstration of SCALES on a heterostructured Si/Ge nanowire. (a) SEM image of a representative as-grown Si/Ge nanowire. Si and Ge segments are false-colored red and blue, respectively. (b) SEM image of a representative Si/Ge nanowire following KOH treatment. KOH is used to remove Si deposited on the Ge segment during nanowire growth. (c) SEM image of a representative PMMA-grafted Si/Ge nanowire. PMMA is false-colored green for clarity. (d) SEM image of a representative PMMA-grafted Si/Ge nanowire following H₂O₂ etching. PMMA is removed from the Ge segment, but remains on the Si. Scale bar, 100 nm. The original, uncolored SEM images are shown in Figure S5.

densities and short to moderate chain lengths are known to reduce chain entanglement, ⁴² resulting in the more facile solvation and removal of the polymer following cleavage from the substrate. Low graft densities and long chains likely have the opposite effect. This situation would lead to cross-film entanglement that reduces the achievable spatial resolution. Knowledge of etchant diffusion through the polymer brush is also essential to improve the SCALES process but has not been widely studied because there was little motivation to do so in the past. Moreover, future research should leverage nanoscale characterization techniques such as atomic force microscopy-based infrared spectroscopy to gain detailed knowledge of local bonding variations at various points during the process. ⁴³

The SCALES process is a versatile route to mask micro/nanostructures, simply requiring (1) initial compositional heterogeneity, (2) an ability to attach a suitable polymer, and (3) an etchant that is selective to one composition but not

the other. The VLS mechanism is an ideal synthetic method to explore SCALES because of its ability to bottom-up encode composition along the length of semiconductor nanowires. In this study, we demonstrate the process on group IV substrates and nanowires because of the availability of both surface grafting methods and selective etchants for Si (SiO_x) and Ge (GeO_x) . However, we emphasize that a variety of top-down and bottom-up fabricated structures are likely amenable to SCALES. For example, we see opportunities to apply SCALES to group III–V materials for which axial composition modulation in nanowires is now commonplace 44,45 and some selective etchants are already known. The is worth noting that the surface chemistry for attachment and grafting may be different in these cases and that distinct attachment methods and etch chemistries will need to be developed and explored.

CONCLUSION

We introduce and demonstrate the SCALES process for bottom-up masking Si/Ge substrates and nanowires. SCALES is a three-step process starting with the encoding of compositional heterogeneity, followed by a blanket surface-initiated polymerization, and completed with a selective etch that removes the polymer brush only from a desired surface. We have investigated the time scale for selective etching on planar Si and Ge surfaces with XPS and ellipsometry and characterized the SCALES process on Si/Ge nanowires with SEM. Our approach is especially useful for creating polymer masks on nanowires, where chemical heterogeneity can be encoded from the bottom-up. Although the present demonstration focuses on Si/Ge nanowires, SCALES is compatible with the many nanowire material systems where compositional modulation is commonplace.

METHODS

Substrate Preparation. Planar substrates are cut into 3 cm × 3 cm squares from Si(111) (El-Cat, 10–55 Ω -cm, double-side polished, phosphorus-doped) or Ge(111) (MTI Corp., 50 Ω -cm, double-side polished, undoped) wafers. Prior to polymerization, all substrates/nanostructures are sequentially cleaned in acetone (99.5%, VWR), methanol (99.8%, VWR), and a 10 vol % NH₄OH (28–30%, Sigma-Aldrich) in deionized (DI) water solution, followed by a DI water rinse. Substrates for nanowire growth are prepared by depositing gold colloid (Ted Pella, 100 nm) on 200 nm of thermally grown SiO₂ on Si(100) substrates (University Wafer, 1–10 Ω -cm, single-side polished, boron-doped). 3-Aminopropyltriethoxysilane (APTES, Sigma-Aldrich, 99%) is used as an adhesion mediator for the gold colloid.⁴⁷

Nanowire Growth. Si, Ge, and Si/Ge nanowires are synthesized in a cold-wall chemical vapor deposition reactor⁴⁸ (FirstNano, Easy Tube 3000) with different combinations of silane (Voltaix, SiH₄, 99.99%), germane (Matheson Tri-Gas, GeH₄, 99.99%), hydrogen bromide (Matheson Tri-Gas, HBr, 99.99%), and hydrogen (AirGas, H₂, 99.99%). For homogeneous Si nanowires, nucleation occurs at 500 °C for 2 min followed by elongation at 480 °C for 10 min in the presence of 1000 sccm H2 and 100 sccm SiH4 at 10 Torr total pressure. For homogeneous Ge nanowires, nucleation occurs at 380 °C for 2 min followed by elongation at 270 °C for 10 min in the presence of 100 sccm H₂ and 30 sccm GeH₄ at 2 Torr total pressure. Si/Ge heterostructured nanowires are grown via methods adapted from the literature. 4,49 A Ge segment is first grown using the above procedure. Upon completion of Ge segment growth, the GeH4 supply is terminated, and the substrate temperature is increased from 270 °C to 430 °C with 10 sccm HBr. HBr passivates the Ge segment sidewalls, minimizing motion and diffusion of the gold seed particle during heating. S,S0,S1 Upon reaching 430 $^{\circ}$ C, 30 sccm SiH₄ is delivered for 5 min at 2.8 Torr total pressure.

Surface-Initiated Polymerization. Figure 1 shows our surfaceinitiated polymerization scheme, 25 including (1) covalent attachment of an anchoring group, (2) covalent attachment of an initiator to the anchoring group, and (3) surface-initiated polymerization from the initiator. All polymerization steps occur in a nitrogen-purged glovebox (OMNI-LAB) and are the same for all substrates and nanowires. APTES is initially attached using a 0.1% v/v anhydrous toluene (Sigma-Aldrich, 99.8%) solution at 70 °C for 20 min. 29,52,53 Attachment of bromoisobutyryl bromide (BIBB, Sigma-Aldrich, 98%), a tertiary bromide polymerization initiator, is accomplished via reaction of APTES-terminated surfaces with a 2:1:12 mixture by volume of BIBB, triethylamine (Sigma-Aldrich, 99.5%), and toluene at room temperature for 2 $h.^{21,24}$ ATRP polymerization of PMMA is carried out by first mixing CuBr (98%, Sigma-Aldrich), CuBr₂ (Sigma-Aldrich, 99%), and 2,2'-bipyridyl (bpy, Sigma-Aldrich, 99%) in a ratio of 1:0.7:4.7 by weight, to which 0.5 mL of anhydrous dimethylformamide (Sigma-Aldrich, 99.8%) and 3.8 mL of methyl methacrylate (MMA, Sigma-Aldrich, 99%) are then added. This mixture is heated to 100 °C, the BIBB-coated substrates/nanowires are added, and PMMA polymerization is carried out for 4 h.

Selective Etching. PMMA-covered substrates/nanowires are removed from the glovebox and immersed in isopropyl alcohol (VWR, 99%) for 30 min. After drying, selective etching is completed by immersing the substrates/nanowires in a 10 vol % $\rm H_2O_2$ (Sigma-Aldrich, 30% in $\rm H_2O$) in DI water solution for 10–60 min. After the desired etch time, the substrates are placed in isopropyl alcohol for 30 min to remove residual polymer.

Characterization. On planar Si and Ge substrates, polymer thickness is determined by ellipsometry (Woollam M2000 ellipsometer) using a standard Cauchy film model for PMMA. Polymer removal is corroborated using XPS (Thermo K-Alpha, Al K alpha source, spot size 400 μ m, pass energy 50 eV). An electron flood gun is used for charge compensation. It is important to make two points about XPS in the context of the present work. Foremost, there is no obvious internal standard with which to correct raw peak positions. The Si(2p) and Ge(3d) photoelectron peak intensities are weak for polymer-covered surfaces, and the C(1s) photoelectron peak of adventitious carbon is hidden within the C(1s) envelope of PMMA. As a result, we chose to show uncorrected spectra but also note that polymer thickness does not strongly impact photoelectron peak position (Supporting Information, Figure S6). Moreover, a measurement of polymer removal during etching assumes integrated peak intensities, and thus photoelectron cross sections, that do not depend on charging. Such behavior is commonly observed for similar systems, and we assume it to be the case in the present work.³² In the case of Si, Ge, and Si/Ge nanowires, nanowire structure and polymer layer morphology are tracked with scanning electron microscopy (SEM, Hitachi SU-8230) at each step. Additional structural and compositional information for Ge nanowires is obtained using STEM (Hitachi HD-2700) with a 0.1 nm resolution at 200 keV. Nanowires were transferred to carbon-coated grids (Ted Pella) by direct mechanical transfer.

ASSOCIATED CONTENT

S Supporting Information

The Supporting Information is available free of charge at https://pubs.acs.org/doi/10.1021/acsnano.9b04363.

Raw C(1s) and Si(2p)/Ge(3d) spectra for transient etching studies; non-false-colored SEM images of the homogeneous Si/Ge nanowires; STEM and EDX images of the polymer-removed Ge nanowire; non-false-colored SEM images of the heterostructured Si/Ge nanowires; and XPS spectra for thickness trials (PDF)

AUTHOR INFORMATION

Corresponding Author

*E-mail: michael.filler@chbe.gatech.edu.

ORCID ®

Eric M. Vogel: 0000-0002-6110-1361 Michael A. Filler: 0000-0003-4239-8558

Notes

The authors declare no competing financial interest.

ACKNOWLEDGMENTS

We would like to thank the National Science Foundation for their financial support (CBET-1604931 and CBET-1916953). Part of the work at the Georgia Institute of Technology was performed at the Institute for Electronics and Nanotechnology (IEN), a member of the National Nanotechnology Coordinated Infrastructure supported by the National Science Foundation through grant ECCS-1542174. We specifically thank the staff of the IEN, most notably Vinh Nguyen for maintaining our CVD system and Mengkun Tian for assistance with STEM.

REFERENCES

- (1) Dasgupta, N. P.; Sun, J.; Liu, C.; Brittman, S.; Andrews, S. C.; Lim, J.; Gao, H.; Yan, R.; Yang, P. 25th Anniversary Article: Semiconductor Nanowires Synthesis, Characterization, and Applications. *Adv. Mater.* **2014**, *26*, 2137–2184.
- (2) Ek, M.; Filler, M. A. Atomic-Scale Choreography of Vapor-Liquid-Solid Nanowire Growth. Acc. Chem. Res. 2018, 51, 118–126.
- (3) Wagner, R. S.; Ellis, W. C. Vapor-Liquid-Solid Mechanism of Single Crystal Growth. *Appl. Phys. Lett.* **1964**, *4*, 89–90.
- (4) Dayeh, S. A.; Wang, J.; Li, N.; Huang, J. Y.; Gin, A. V.; Picraux, S. T. Growth, Defect Formation, and Morphology Control of Germanium-Silicon Semiconductor Nanowire Heterostructures. *Nano Lett.* **2011**, *11*, 4200–4206.
- (5) Hui, H.; De La Mata, M.; Arbiol, J.; Filler, M. A. Low-Temperature Growth of Axial Si/Ge Nanowire Heterostructures Enabled by Trisilane. *Chem. Mater.* **2017**, *29*, 3397–3402.
- (6) Pinion, C. W.; Christesen, J. D.; Cahoon, J. F. Understanding the Vapor–Liquid–Solid Mechanism of Si Nanowire Growth and Doping to Synthetically Encode Precise Nanoscale Morphology. *J. Mater. Chem. C* **2016**, *4*, 3890–3897.
- (7) Lu, W.; Xie, P.; Lieber, C. M. Nanowire Transistor Performance Limits and Applications. *IEEE Trans. Electron Devices* **2008**, *55*, 2859–2876.
- (8) Patolsky, F.; Zheng, G.; Lieber, C. Nanowire-Based Biosensors. *Anal. Chem.* **2006**, 78, 4260–4269.
- (9) Armelles, G.; Cebollada, A.; Garcia-Martin, A.; Montero-Moreno, J. M.; Waleczek, M.; Nielsch, K. Magneto-Optical Properties of Core-Shell Magneto-Plasmonic Au-Co(x)Fe(3 x)O4 Nanowires. *Langmuir* **2012**, *28*, 9127–9130.
- (10) Wallentin, J.; Anttu, N.; Asoli, D.; Huffman, M.; Aberg, I.; Magnusson, M. H.; Siefer, G.; Fuss-Kailuwet, P.; Dimroth, F.; Witzigmann, B.; Xu, H. Q.; Samuelson, L.; Deppert, K.; Borgstrom, M. T. InP Nanowire Array Solar Cells Achieving 13.8% Efficiency by Exceeding the Ray Optics Limit. *Science* 2013, 339, 1057–1060.
- (11) Behrens, S. H.; Breedveld, V.; Mujica, M.; Filler, M. A. Process Principles for Large-Scale Nanomanufacturing. *Annu. Rev. Chem. Biomol. Eng.* **2017**, *8*, 201–226.
- (12) George, S. M. Atomic Layer Deposition: An Overview. *Chem. Rev.* **2010**, *110*, 111–131.
- (13) Johnson, R. W.; Hultqvist, A.; Bent, S. F. A Brief Review of Atomic Layer Deposition: From Fundamentals to Applications. *Mater. Today* **2014**, *17*, 236–246.
- (14) Mackus, A. J.; Bol, A. A.; Kessels, W. M. The Use of Atomic Layer Deposition in Advanced Nanopatterning. *Nanoscale* **2014**, *6*, 10941–10960.
- (15) Park, K. J.; Doub, J. M.; Gougousi, T.; Parsons, G. N. Microcontact Patterning of Ruthenium Gate Electrodes by Selective Area Atomic Layer Deposition. *Appl. Phys. Lett.* **2005**, *86*, 1–4.

(16) Namazi, L.; Nilsson, M.; Lehmann, S.; Thelander, C.; Dick, K. A. Selective GaSb Radial Growth on Crystal Phase Engineered InAs Nanowires. *Nanoscale* **2015**, *7*, 10472–10481.

- (17) Singh, J. A.; Thissen, N. F. W.; Kim, W. H.; Johnson, H.; Kessels, W. M. M.; Bol, A. A.; Bent, S. F.; Mackus, A. J. M. Area-Selective Atomic Layer Deposition of Metal Oxides on Noble Metals through Catalytic Oxygen Activation. *Chem. Mater.* **2018**, *30*, 663–670
- (18) Farm, E.; Kemell, M.; Ritala, M.; Leskela, M. Selective-Area Atomic Layer Deposition Using Poly(Methyl Methacrylate) Films as Mask Layers. *J. Phys. Chem. C* **2008**, *112*, 15791–15795.
- (19) Hashemi, F. S.; Prasittichai, C.; Bent, S. F. Self-Correcting Process for High Quality Patterning by Atomic Layer Deposition. *ACS Nano* **2015**, *9*, 8710–8717.
- (20) Sneh, O.; Clark-Phelps, R. B.; Londergan, A. R.; Winkler, J.; Siedel, T. E. Thin Film Atomic Lyer Deposition Equipment for Semiconductor Processing. *Thin Solid Films* **2002**, 402, 248–261.
- (21) Bansal, A.; Kumar, A.; Kumar, P.; Bojja, S.; Chatterjee, A. K.; Ray, S. S.; Jain, S. L. Visible Light-Induced Surface Initiated Atom Transfer Radical Polymerization of Methyl Methacrylate on Titania/Reduced Graphene Oxide Nanocomposite. *RSC Adv.* **2015**, *5*, 21189–21196.
- (22) Kwak, Y.; Matyjaszewski, K. ARGET ATRP of Methyl Methacrylate in the Presence of Nitrogen-Based Ligands as Reducing Agents. *Polym. Int.* **2009**, *58*, 242–247.
- (23) Matyjaszewski, K. Atom Transfer Radical Polymerization (ATRP): Current Status and Future Perspectives. *Macromolecules* **2012**, *45*, 4015–4039.
- (24) Minet, I.; Delhalle, J.; Hevesi, L.; Mekhalif, Z. Surface-Initiated ATRP of PMMA, PS and Diblock PS-b-PMMA Copolymers from Stainless Steel Modified by 11-(2-Bromoisobutyrate)-Undecyl-1-Phosphonic Acid. *J. Colloid Interface Sci.* **2009**, 332, 317–326.
- (25) Zhang, H.; Jiang, Y.; Yu, Q. Grafting Polymer Brushes from Glass Fibers by Surface-Initiated ATRP. *Macromol. React. Eng.* **2010**, 4, 251–256.
- (26) Ardalan, P.; Sun, Y.; Pianetta, P.; Musgrave, C. B.; Bent, S. F. Reaction Mechanism, Bonding, and Thermal Stability of 1-Alkanethiols Self-Assembled on Halogenated Ge Surfaces. *Langmuir* **2010**, *26*, 8419–8429.
- (27) Onsia, B.; Conard, T.; De Gendt, S.; Heyns, M. M.; Hoflijk, I.; Mertens, P. W.; Meuris, M.; Raskin, G.; Sioncke, S.; Teerlinck, I.; Theuwis, J.; Vinckier, C. Study of the Influence of Typical Wet Chemical Treatments on the Germanium Wafer Surface. *Solid State Phenom.* 2005, 103-104, 19–22.
- (28) Martin, H.; Schulz, K.; Bumgardner, J.; Walters, K. XPS Study on the Use of 3-Aminopropyltriethoxysilane to Bond Chitosan to a Titanium Surface. *Langmuir* **2007**, *23*, 6645–6651.
- (29) Acres, R. G.; Ellis, A. V.; Alvino, J.; Lenahan, C. E.; Khodakov, D. A.; Metha, G. F.; Andersson, G. G. Molecular Structure of 3-Aminopropyltriethoxysilane Layers Formed on Silanol-Terminated Silicon Surfaces. J. Phys. Chem. C 2012, 116, 6289–6297.
- (30) Chen, Z.; Xie, L.; Huang, X.; Li, S.; Jiang, P. Achieving Large Dielectric Property Improvement in Polymer/Carbon Nanotube Composites by Engineering the Nanotube Surface *via* Atom Transfer Radical Polymerization. *Carbon* **2015**, *95*, 895–903.
- (31) Klemberg-Sapieha, J. E.; Martinu, L.; Yamasaki, N. L. S.; Lantman, C. W. Tailoring the Adhesion of Optical films on Polymethyl-Methacrylate by Plasma-Induced Surface Stabilization. *Thin Solid Films* **2005**, 476, 101–107.
- (32) Ton-That, C.; Shard, A. G.; Teare, D. O. H.; Bradley, R. H. XPS and AFM Surface Studies of Solvent-Cast PS/PMMA Blends. *Polymer* **2001**, 42, 1121–1129.
- (33) Louette, P.; Bodino, F.; Pireaux, J. Poly(Methyl Methacrylate) (PMMA) XPS Reference Core Level and Energy Loss Spectra. Surf. Sci. Spectra 2005, 12, 69–73.
- (34) Sioncke, S.; Brunco, D. P.; Meuris, M.; Uwamahoro, O.; Van Steenbergen, J.; Vrancken, E.; Heyns, M. M. Etch Rate Study of Germanium, GaAs and InGaAs: A Challenge in Semiconductor Processing. *Solid State Phenom.* **2009**, *145-146*, 203–206.

- (35) Yu, Y.; Kieviet, B. D.; Kutnyanszky, E.; Vancso, G. J.; de Beer, S. Cosolvency-Induced Switching of the Adhesion between Poly-(Methyl Methacrylate) Brushes. *ACS Macro Lett.* **2015**, *4*, 75–79.
- (36) Büttner, C. C.; Zakharov, N. D.; Pippel, E.; Gösele, U.; Werner, P. Gold-Enhanced Oxidation of MBE-Grown Silicon Nanowires. *Semicond. Sci. Technol.* **2008**, 23, 1–6.
- (37) Groele, R. J.; Krasicky, P. D.; Chun, S. W.; Sullivan, J.; Rodriguez, F. Dissolution Rates of Poly(methyl Methacrylate) in Mixtures of Nonsolvents. *J. Appl. Polym. Sci.* **1991**, *42*, 3–8.
- (38) Gunji, M.; Thombare, S. V.; Hu, S.; McIntyre, P. C. Directed Synthesis of Germanium Oxide Nanowires by Vapor-Liquid-Solid Oxidation. *Nanotechnology* **2012**, *23*, 1–6.
- (39) Xie, T.; Schmidt, V.; Pippel, E.; Senz, S.; Gosele, U. Gold-Enhanced Low-Temperature Oxidation of Silicon Nanowires. *Small* **2008**, *4*, 64–68.
- (40) Xu, T.; Nys, J. P.; Addad, A.; Lebedev, O. I.; Urbieta, A.; Salhi, B.; Berthe, M.; Grandidier, B.; Stiévenard, D. Faceted Sidewalls of Silicon Nanowires: Au-Induced Structural Reconstructions and Electronic Properties. *Phys. Rev. B: Condens. Matter Mater. Phys.* **2010**, *81*, 1–10.
- (41) Leancu, R.; Moldovan, N.; Csepregi, L.; Lang, W. Anisotropic Etching of Germanium. Sens. Actuators, A 1995, 46–47, 35–37.
- (42) Choi, J.; Hui, C. M.; Pietrasik, J.; Dong, H.; Matyjaszewski, K.; Bockstaller, M. R. Toughening Fragile Matter: Mechanical Properties of Particle Solids Assembled from Polymer-Grafted Hybrid Particles Synthesized By ATRP. *Soft Matter* **2012**, *8*, 4072–4082.
- (43) Dazzi, A.; Prater, C. B. AFM-IR: Technology and Applications in Nanoscale Infrared Spectroscopy and Chemical Imaging. *Chem. Rev.* 2017, 117, 5146–5173.
- (44) Caroff, P.; Dick, K. A.; Johansson, J.; Messing, M. E.; Deppert, K.; Samuelson, L. Controlled Polytypic and Twin-Plane Superlattices in III-V Nanowires. *Nat. Nanotechnol.* **2009**, *4*, 50–55.
- (45) Cirlin, G. E.; Reznik, R. R.; Shtrom, I. V.; Khrebtov, A. I.; Samsonenko, Yu B.; Kukushkin, S. A.; Kasama, T.; Akopian, N.; Leonardo, L. Hybrid GaAs/AlGaAs Nanowire—Quantum Dot System for Single Photon Sources. *Semiconductors* **2018**, *52*, 462–464.
- (46) Clawson, A. R. Guide to References on III-V Semiconductor Chemical Etching. *Mater. Sci. Eng., R* **2001**, *31*, 1–438.
- (47) Woodruff, J. H.; Ratchford, J. B.; Goldthorpe, I. A.; McIntyre, P. C.; Chidsey, E. D. C. Vertically Oriented Germanium Nanowires Grown from Gold Colloids on Silicon Substrates and Subsequent Gold Removal. *Nano Lett.* **2007**, *7*, 1637–1642.
- (48) Musin, I. R.; Filler, M. A. Chemical Control of Semiconductor Nanowire Kinking and Superstructure. *Nano Lett.* **2012**, *12*, 3363–3368.
- (49) Periwal, P.; Baron, T.; Gentile, P.; Salem, B.; Bassani, F. Growth Strategies to Control Tapering in Ge Nanowires. *APL Mater.* **2014**, *2*, 1–8.
- (50) Sivaram, S. V.; Shin, N.; Chou, L. W.; Filler, M. A. Direct Observation of Transient Surface Species during Ge Nanowire Growth and Their Influence on Growth Stability. *J. Am. Chem. Soc.* **2015**, *137*, 9861–9689.
- (51) D'Evelyn, M. P.; Yang, Y. L.; Cohen, S. M. Adsorption, Desorption, and Decomposition of HCl and HBr on Ge(100): Competitive Pairing and Near-First-Order Desorption Kinetics. *J. Chem. Phys.* **1994**, *101*, 2463–2475.
- (52) Pasternack, R. M.; Amy, S. R.; Chabal, Y. J. Attachment of 3-(Aminopropyl)triethoxysilane on Silicon Oxide Surfaces: Dependence on Solution Temperature. *Langmuir* **2008**, *24*, 12963–12971.
- (53) Vandenberg, E. T.; Bertilsson, L.; Liedberg, B.; Uvdal, K.; Erlandsson, R.; Elwing, H.; Lundstrom, I. Structure of 3-Aminopropyl Triethoxy Silane on Silicon Oxide. *J. Colloid Interface Sci.* **1991**, *147*, 103–118.